Electronic structure of layered quaternary chalcogenide materials for band-gap engineering: The example of $Cs_2M^{II}M_3^{IV}Q_8$

Rafael Besse and Fernando P. Sabino
São Carlos Institute of Physics, University of São Paulo, PO Box 369, 13560-970, São Carlos, São Paulo, Brazil

Juarez L. F. Da Silva*
São Carlos Institute of Chemistry, University of São Paulo, PO Box 780, 13560-970, São Carlos, São Paulo, Brazil

(Received 9 February 2016; revised manuscript received 20 March 2016; published 22 April 2016)

Quaternary chalcogenide materials offer a wide variety of chemical and physical properties, and hence, those compounds have been widely studied for several technological applications. Recently, experimental studies have found that the chalcogenide $Cs_2M^{II}M_3^{IV}Q_8$ family (M^{II} = Mg, Zn, Cd, Hg, M^{IV} = Ge, Sn and Q = S, Se, Te), which includes 24 compounds, yields a wide range of band gaps, namely, from 1.07 to 3.4 eV, and hence, they have attracted great interest. To obtain an improved atomistic understanding of the role of the cations and anions on the physical properties, we performed a first-principles investigation of the 24 $Cs_2M^{II}M_3^{IV}Q_8$ compounds employing density functional theory within semilocal and hybrid exchange-correlation energy functionals and the addition of van der Waals corrections to improve the description of the weakly interacting layers. Our lattice parameters are in good agreement with the available experimental data (i.e., 11 compounds), and the equilibrium volume increases linearly by increasing the atomic number of the chalcogen, which can be explained by the increased atomic radius of the chalcogen atoms from S to Te. We found that van der Waals corrections play a crucial role in the lattice parameter in the stacking direction of the $Cs_2M^{II}M_3^{IV}Q_8$ layers, while the binding energy per unit area has similar magnitude as obtained for different layered materials. We obtained that the band gaps follow a linear relation as a function of the unit cell volume, which can be explained by the atomic size of the chalcogen atom and the relative position of the Q p states within the band structure. The fundamental and optical band gaps differ by less than 0.1 eV. The band gaps obtained with the hybrid functional are in good agreement with the available experimental data. Furthermore, we found from the Bader analysis, that the Coulomb interations among the cations and anions play a crucial role on the energetic properties.

DOI: 10.1103/PhysRevB.93.165205

I. INTRODUCTION

Chalcogenide compounds, in which the chemical composition consists of at least one chalcogen anion, Q, (Q = S, Se, Te) and one or more cation atoms (e.g., alkali metals, alkaline earth metals, transition-metals, etc.) have attracted great interest due to the wide range of existing and potential technological applications [1–3]. For example, thin film heterojunctions of CdTe and CdS have been extensively investigated for applications in photovoltaic devices because of the nearly ideal band gap E_g of CdTe for solar cells (E_g = 1.50 eV), high optical CdTe absorption coefficient, suitable band-gap alignments of CdTe and CdS, cost effective techniques for production at large scale, and stability against proton/electron irradiation [1,4,5]. Furthermore, copper based chalcogenides have been extensively studied also for photovoltaic applications due to optimal band-gap values, absorption coefficients, and as a conductive back-contact for CdTe solar cells [6–8].

The study of binary chalcogenides has provided important contributions to the development of renewable energy technologies, however, the exploration of ternary and quaternary chalcogenide compounds has opened a wide range of new possibilities. For example, $Cs_2Hg_6S_7$, $Cs_2Hg_3Se_4$, and $Cs_2Cd_3Te_4$ have been suggested as potential materials for high-energy radiation detection due to the wide range of band gaps obtained by the combination of chalcogen atoms with cation elements with high average atomic number [9–13]. Beyond of that, chalcogenide compounds such as $LiAsS_2$, and $NaAsSe_2$ have been studied for nonlinear optics [14,15], while the combination of GeTe with Sb_2Te_3 at different compositions has been employed for optical storage devices and have been considered as candidates for nonvolatile memories [2,16–19].

Thus there is a great interest to identify new chalcogenide compounds to tune the physical and chemical properties as a function of the anion and cation compositions. Recently, the quaternary chalcogenides $A_2M^{II}M_3^{IV}Q_8$ family (A = K, Cs, M^{II} = Mg, Zn, Cd, Hg; M^{IV} = Ge, Sn, Q = S, Se, Te), which can yield 48 compounds, was proposed [20,21]. Although 48 compounds can be obtained from the $A_2M^{II}M_3^{IV}Q_8$ family, only 12 compounds were synthesized and characterized by experimental techniques [20,21], which indicates the challenges in the synthesis of chalcogenides. Based on the experimental results [21], they obtained that the 11 studied $Cs_2M^{II}M_3^{IV}Q_8$ compounds, except $Cs_2ZnGe_3S_8$, share the same orthorhombic crystal structure, in which $Cs_2M^{II}M_3^{IV}Q_8$ forms layered structures with a stacking along the b direction. The band gaps change from 1.07 to 3.38 eV, which turns the chalcogenides $Cs_2M^{II}M_3^{IV}Q_8$ family suitable candidate for a wide range of applications. Furthermore, they reported density functional theory (DFT) calculations within the local-density approximation (LDA) for few selected systems [21], however, DFT-LDA cannot provide a correct description of the magnitude of the band gaps and an accurate description of the weak van der Waals (vdW) interactions in layered materials [22–25].

*juarez_dasilva@iqsc.usp.br

Although several properties have been characterized as a function of the chalcogen species, our atomistic understanding of the role of the cation (A, M^{II}, M^{IV}) and anion (Q) atoms in the $A_2M^{II}M_3^{IV}Q_8$ family is far from complete, in particular, due to the challenges to perform the synthesis and characterization for a wide range of compounds and to obtain a reliable theoretical description of the structural, energetic, electronic, and optical properties of chalcogenide layered materials beyond local or semilocal functionals.

In this work, we performed first-principles DFT calculations employing semilocal and hybrid exchange-correlation (XC) energy functionals within vdW corrections to improve our atomistic understanding of the role of the cation and anion atoms in the structural, energetic, electronic, and optical properties of the chalcogenides $Cs_2M^{II}M_3^{IV}Q_8$ family, including all the 24 compounds. We found that the lattice parameters are in good agreement with the available experimental data for 11 compounds [21], and the equilibrium volume increases linearly by increasing the atomic number of the chalcogen, i.e., from S to Te, which can be explained by the increased atomic radius of the chalcogen atoms. The vdW corrections play a crucial role in the lattice parameter in the stacking direction of the $Cs_2M^{II}M_3^{IV}Q_8$ layers, while the binding energy per unit area has similar magnitude as obtained for different layered materials. We obtained that the band gaps follow a linear relation as a function of the unit cell volume, which can be explained by the atomic size of the chalcogen atom and the relative position of the Q p states within the band structure. Beyond of that, band gaps obtained with the hybrid functional are in good agreement with the available experimental data [21].

II. THEORETICAL APPROACH AND COMPUTATIONAL DETAILS

A. Total energy calculations

Our calculations are based on DFT [26,27] within the semilocal generalized gradient approximation (GGA) proposed by Perdew–Burke–Ernzerhof (PBE) [28] to the XC functional. GGA functionals yield an excellent description of a wide range of compounds [29–31], however, semilocal functionals have deficiencies to describe particular systems or properties. For example, a correct description of the structural, energetic, and electronic properties of layered materials (e.g., the phase change $GeTe-Sb_2Te_3$ materials [18]) or physisorption systems on surfaces (e.g., rare-gas adsorption on surfaces [32–34]) is a challenge to DFT-PBE calculations due to the weak long-range nonlocal vdW interactions among the layers and the adsorbed-surface interface, which are poorly described by plain DFT calculations [22–25]. Thus, to improve the description of layered systems such as the $Cs_2M^{II}M_3^{IV}Q_8$ compounds, we employed the vdW correction proposed by Tkatchenko-Scheffler with self-consistent screening (TS+SCS) effects [35,36]. Furthermore, it is well known that DFT within local or semilocal functionals underestimates the magnitude of the band gap in semiconductors [29,37]. Thus, to obtain improved band-gap values, which has great importance for band-gap engineering [9,38], we employed the hybrid functional proposed by Heyd-Scuseria-Ernzerhof (HSE06) [39–41] with a Coulomb screening parameter of 0.206 $Å^{-1}$ and 25% of exact nonlocal Fock exchange in the short-range term [42].

The Kohn-Sham equations were solved using the projector augmented-wave (PAW) method [43,44], as implemented in the Vienna *ab initio* simulation package (VASP) [45,46]. The Kohn-Sham orbitals are expanded in a plane waves basis set with a cutoff energy of 492 eV for stress tensor calculations (e.g., to obtain the equilibrium volumes) due to the slow convergence of the stress tensor as a function of the number of plane waves, while to obtain the total energy, Bader charge, density of states (DOS), band structure, and optical properties, the cutoff energy was set to 369 eV. Due to the large size of the bulk unit cell, for the Brillouin zone integration, we employed a **k**-point mesh of $3\times3\times1$ (2 irreducible **k** points) for $Cs_2CdGe_3S_8$ to compute the structural parameters, however, a **k**-point mesh of $5\times3\times2$ was employed for the Bader charge, DOS, band structure, and optical properties calculations. For all the remaining 23 chalcogenide compounds, the same **k**-point density of $Cs_2CdGe_3S_8$ was employed. To solve the Kohn-Sham equations, we employed a total energy convergence criterion of 1×10^{-5} eV, while the optimized geometries were obtained once the atomic forces were smaller than 0.025 eV/Å on every atom.

It has been known that hybrid DFT-HSE06 calculations [47] have a very high computational cost compared with plain DFT calculations, and hence, our DFT-HSE06 calculations were performed only for fixed volume structures obtained with the PBE or PBE+TS+SCS functionals. Furthermore, we obtained that the band gap changes by less than 0.06 eV using only Γ point instead of the $3\times3\times1$ **k**-point mesh for the $Cs_2CdSn_3S_8$, $Cs_2MgGe_3Se_8$, and $Cs_2ZnGe_3Te_8$ compounds. Thus, to reduce the computational cost further, all the DFT-HSE06 band-gap values were obtained using only the Γ point, which does not affect the conclusions obtained in this work.

B. Crystal structures: chalcogenide $Cs_2M^{II}M_3^{IV}Q_8$ family

As defined above, the chalcogenides $Cs_2M^{II}M_3^{IV}Q_8$ family has 24 compounds, however, only 11 of them were synthesized and characterized by experimental techniques [21]. Ten of the 11 studied compounds crystallize in the orthorhombic structure with space group $P2_12_12_1$, while only the $Cs_2ZnGe_3S_8$ compound crystallizes in the monoclinic structure with space group $P2_1/n$ and a γ angle of 97.7°, Fig. 1 [21]. Both structures have four formula units (f.u.) per primitive cell, and are characterized by the stacking of the $Cs_4M_2^{II}M_6^{IV}Q_{16}$ layers along the b axis, Fig. 1. In each layer the Q anions are located in twofold lattice sites, while the cations, M^{II} and M^{IV}, are located in fourfold lattice sites and the Cs cations are located in the high coordination lattice sites, e.g., nine. Thus, we can conclude that the orthorhombic and monoclinic crystal structures differ mainly in the γ angle, which deviates by 7.7° from the orthorhombic structure for $Cs_2ZnGe_3S_8$. Therefore we calculated all the 24 compounds in the orthorhombic crystal structure (i.e., the α, β, and γ angles were restricted to 90° for all calculations). Beyond of that, the $Cs_2ZnGe_3S_8$ system and an extra compound were calculated in the monoclinic structure to check the relative stability among the orthorhombic and monoclinic structures.

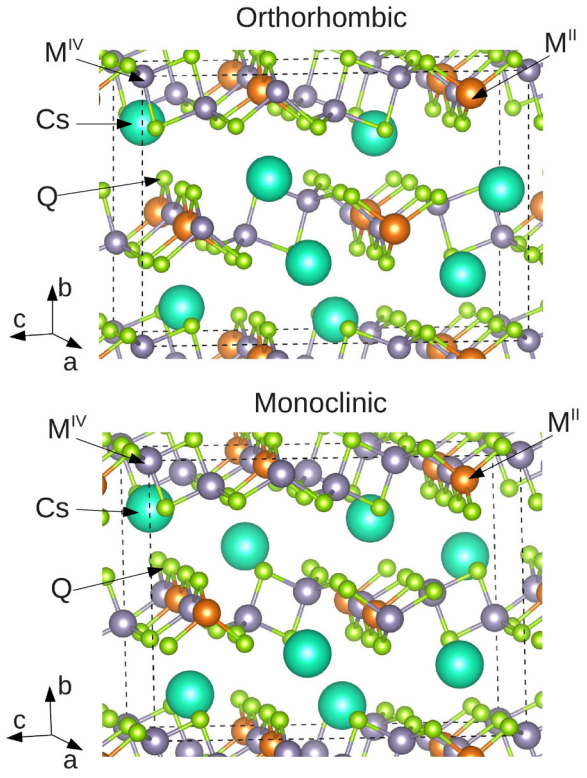

FIG. 1. Representation of the orthorhombic and monoclinic crystal structures of the $Cs_2M^{II}M^{IV}_3Q_8$ compounds, where M^{II} = Mg, Zn, Cd, Hg; M^{IV} = Ge, Sn; Q = S, Se, and Te. The atoms are represented by spheres of different radii, that increase in the sequence Q (green), M^{IV} (purple), M^{II} (orange), and Cs (cyan).

III. RESULTS AND DISCUSSION

Below, we will summarize our results and discussion of the most important structural, energetic, and electronic properties, while several results used to support our discussion and conclusions are summarized in the Supplemental Material (Ref. [49]).

A. Structural properties

The equilibrium lattice parameters of the $Cs_2M^{II}M^{IV}_3Q_8$ compounds in the orthorhombic crystal structure as a function of the chalcogen species, Q, are shown in Fig. 2, while the numerical results are summarized in Table S1 (Ref. [49]). For all systems, the lattice parameters (equilibrium volumes) for a given set of cations (M^{II} and M^{IV}) increase from S to Te, which can be explained by the increased atomic radius, R_c, from S to Te (e.g., the ionic radius are 1.84 Å for S, 1.98 Å for Se, and 2.21 Å for Te) [48]. This trend was also observed experimentally for the studied $Cs_2M^{II}M^{IV}_3Q_8$ compounds [21], as well as for different chalcogenide families, e.g., $Tl_2Hg_3Q_4$ [10,50]. From our analysis based on the $\frac{\Delta a}{\Delta R_c}$ ratio, the effects are larger on the a_0 and c_0 parameters due to the available space between the layers, which absorbs part of the layer expansion, and hence, b_0 is not strongly affected as a_0 and c_0. The equilibrium volume also increases when Ge is replaced by Sn, for fixed M^{II} and Q species, following mainly the increase of the a_0 and c_0 parameters, which can also be explained by the larger ionic radius of Sn (0.71 Å) in comparison with Ge (0.53 Å) [48].

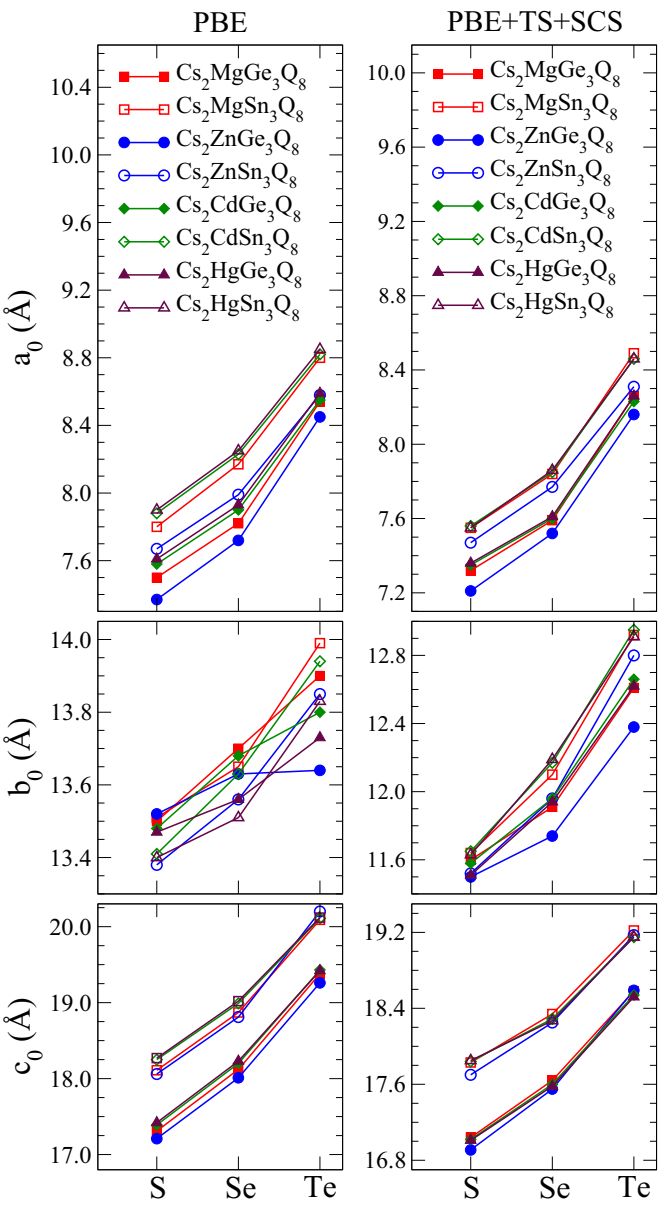

FIG. 2. Equilibrium PBE and PBE+TS+SCS lattice parameters (a_0, b_0, c_0) of the $Cs_2M^{II}M^{IV}_3Q_8$ compounds in the orthorhombic crystal structure, Fig. 1, as a function of the chalcogen species (S, Se, Te).

The addition of the vdW correction does not change the behavior of the equilibrium lattice parameters as a function of the chalcogen atomic number, but affects the magnitude of the lattice parameters, Fig. 2 and Table S1 (Ref. [49]). For example, for all systems, a_0 and c_0 are reduced at an average of 3.6% and 3.4%, respectively, compared with the PBE results, while b_0 is reduced at an average of 11.2%, which can be explained by the attractive nature of the vdW corrections [35,51]. The contractions of a_0 and c_0 in $Cs_2M^{II}M^{IV}_3Q_8$ due to the vdW correction are larger than usualy obtained for layered vdW materials. For example, the lateral lattice parameters contracts by 0.40% for bulk graphite and expands

by 0.43 % for V_2O_5 compared with PBE results [25,36]. This behavior can be explained by the atomic structure of the $Cs_2M^{II}M^{IV}_3Q_8$ layer, which is composed by a zigzag structure, Fig. 2. The vdW correction reduces the angles between the $M^{IV}-Q$ and $M^{II}-Q$ bonds in the linear chains along the a axis and also the angles between different $M^{IV}-Q$ or $M^{II}-Q$ bonds in the linear chains along the c axis, Fig. S3 (Ref. [49]). In comparison with the experimental results (11 compounds) [21], PBE overestimates b_0 from 6.0% to 8.0%, while PBE+TS+SCS underestimates from 4.0% to 8.0%, i.e., similar error bars, but opposite directions. A similar trend is observed for the a_0 and c_0 parameters, however, the magnitude of the relative errors are smaller (e.g., 2.8% for a_0 using PBE and 0.8% using PBE+TS+SCS).

To improve our understanding of the structural properties, we employed the effective coordination concept [52,53], which yields the weighted bond length, d^i_{av}, and the effective coordination number, ECN^i, given in number of nearest neighbors (NNN) for each atom in the unit cell. The average results are summarized in the Tables S2 and S3 (Ref. [49]). We found that $ECN^{M^{II}} \sim 4.0$ NNN for all compounds, where $M^{II}-Q_4$ forms nearly an ideal tetrahedron environment. In contrast, $ECN^{M^{IV}} = 3.94$ to 4.07 NNN, and $M^{IV}-Q_4$ forms slighly distorted tetrahedra due to the differences in the bond lengths and angles. For the Cs atoms, the ECN results are betweem 11.44 NNN and 13.44 NNN, which increases by nearly one unit by the addition of the vdW correction and it can be explained by the decreasing in the b_0 lattice parameter and smaller empty space for the Cs atoms. Based on the d^i_{av} results and the hard-sphere model ($R_a = \frac{d_{av}}{2}$) [54], we calculated the PBE average atomic radius using all 24 compounds, R_a, namely, 1.18 Å for S, 1.25 Å for Se, and 1.37 Å for Te (the remaining results are summarized in Table S4, Ref. [49]). The results follow the same trends of the ionic radius, and hence, it explains the behavior of the lattice parameters as a function of the chalcogen atom, Q.

B. Orthorhombic versus monoclinic structure

To investigate the relative energy stability between the orthorhombic and monoclinic structures [21], we obtained the equilibrium crystal structure of the $Cs_2CdSn_3Se_8$ and $Cs_2ZnGe_3S_8$ compounds in the orthorhombic and monoclinic structures employing the PBE and PBE+TS+SCS functionals. The relative differences between the equilibrium lattice parameters among the two crystal structures are smaller than 3%, and the γ angle of the monoclinic structures deviates from the orthorhombic structure ($\gamma = 90^\circ$) from 0.4° to 3.3°. Beyond of that, the energy differences range from −0.5 meV/atom to 5.5 meV/atom, i.e., they are nearly degenerated. Therefore it can be seen that the two structures have great structural and energetic similarity.

C. Energetic properties

To improve our understanding of the energetic stability, we calculated the cohesive energy E_{coh} with respect to the free atoms in their ground-state spin configurations. The results with and without the vdW correction are shown in Fig. 3, while the numerical values are in Table S7 (Ref. [49]).

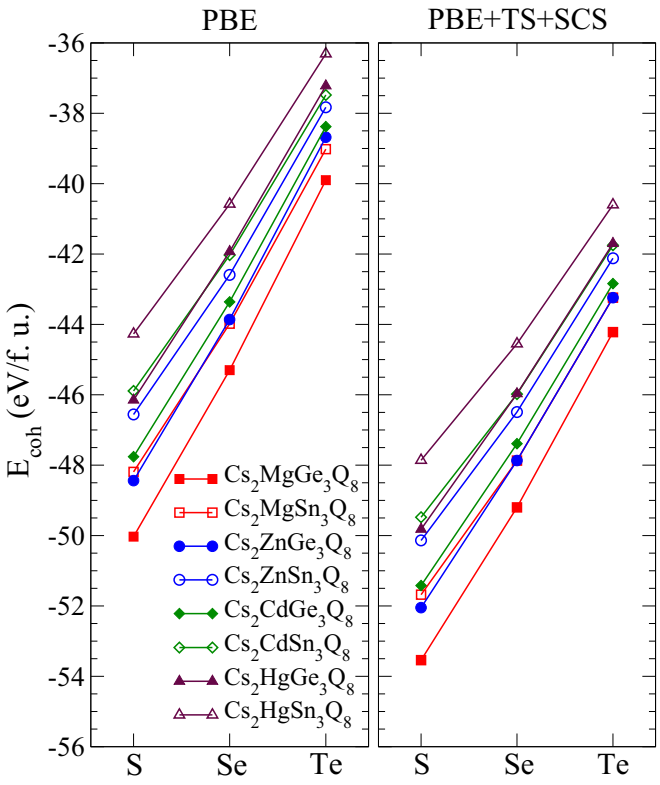

FIG. 3. Cohesive energies of the $Cs_2M^{II}M^{IV}_3Q_8$ compounds for PBE and PBE+TS+TSC as a function of the chalcogen species.

As the vdW correction does not affect the free atom total energy, the differences between PBE and PBE+TS+SCS results are related entirely to the bulk total energy. For both XC functionals, we found that E_{coh} decreases linearly by increasing the atomic radius from S to Te, which is consistent with the trends obtained for the lattice parameters. Furthermore, the atomic size of the M^{II} and M^{IV} plays also an important role.

To evaluate the magnitude of the strength of the interactions between the layers, we calculated the interlayer binding energies for the 24 compounds, with and without the vdW correction. Our results are shown in Fig. 4 and Table S9 (Ref. [49]) and indicate a large increase in the absolute value of interlayer binding energies by the addition of the vdW correction, which is expected due to the attractive nature of the vdW interaction. The interlayer PBE+TS+SCS binding energy is in the range from 15 to 27 meV/Å^2, which is close to the results obtained by Björkman *et al.* [55] employing nonlocal correlation functionals and the random-phase approximation to the study of a large number of layered materials.

To understand the role of the Coulomb interactions in the behavior of the cohesive energy as a function of the atomic radius of the Q, M^{II}, and M^{IV} atoms, we calculated the Bader charges Q_B on every atom [56,57]. The effective charge Q_{eff} on every atom was calculated as follows, $Q_{eff} = Z_{val} - Q_B$, where Z_{val} is the number of valence electrons (i.e., 9 for Cs, 12 for Zn, Cd and Hg, 2 for Mg, 14 for M^{IV}, and 6 for Q). The average Q_{eff} results for each chemical species are shown in Fig. 5, while numerical results are reported in Table S8 (Ref. [49]). The

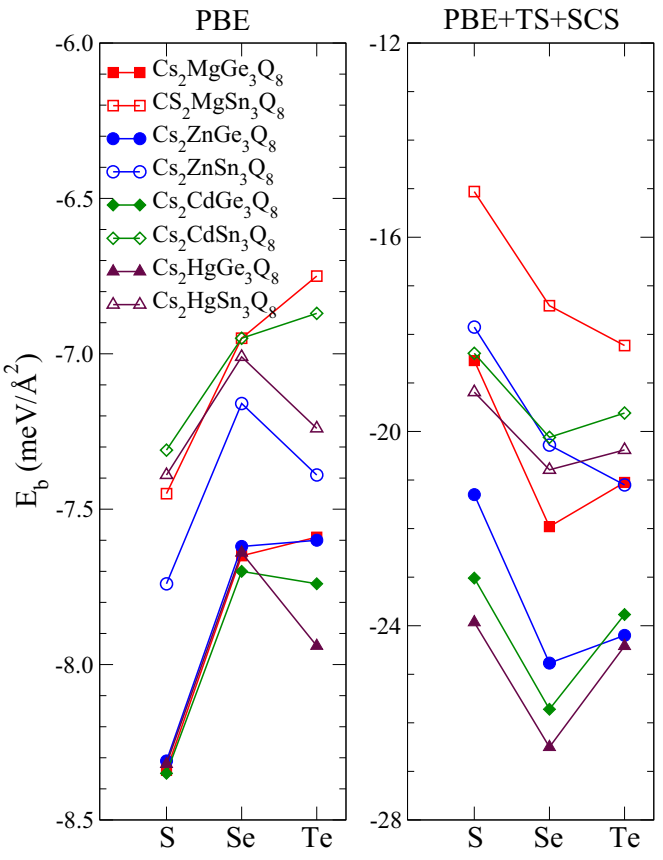

FIG. 4. Interlayer binding energies of the $Cs_2M^{II}M_3^{IV}Q_8$ compounds for PBE and PBE+TS+SCS as a function of the chalcogen species.

effective charges obtained with PBE+TS+SCS share the same trends and have slightly smaller absolute values compared with the PBE results, so that the increase in the magnitude of the repulsive interactions due to the shorter distances between ions with same charge sign are compensated by this decrease of the ionic character.

We found that the Cs, M^{II}, and M^{IV} atoms donate charge to the chalcogen atoms, which is expected based on the Pauling electronegativity concept ($\chi = 2.58$ for S, 2.55 for Se, and 2.1 for Te) [58]. The magnitude of the effective Bader charges is related with the magnitude of the electronegativity differences. For example, the absolute ionic charge on Q increases almost linearly from Te to S, while the effective charge on the cations (Cs, M^{II}, and M^{IV}) decreases from S to Te. Thus the magnitude of the Coulomb interactions decrease from S to Te, and hence, it can explain the trends in the cohesive energy, i.e., larger effective charges in the anions and cations increase the Coulomb interactions, which helps to stabilize the system by increasing the cohesive energy and reducing the lattice parameters. Therefore the ionic character in those chalcogenide systems plays a crucial role in the stability properties of the $Cs_2M^{II}M_3^{IV}Q_8$ compounds.

D. Electronic properties

To characterize the electronic states, we obtained the electronic density of states (DOS), which is shown in Fig. 6 for the selected $Cs_2CdGe_3Q_8$ compounds, while the general characteristics of the DOS of the remaining compounds are very similar (Figs. S4 to S10 in Ref. [49]). The valence band maximum and its vicinity are composed mainly by Q p states. In contrast, the conduction band minimum is composed by M^{IV} s states and Q p states. Furthermore, the substitution of Ge by Sn increases the localization of all the states as a result of increasing the atomic radii and consequently the bond lengths. We found that the spread of the electronic states is affected by the vdW correction, which is expected due to the reduction of the interlayer distance, and hence, an increase in the orbital overlap of the states, see also Fig. S11 in Ref. [49].

The PBE band structures for $Cs_2CdGe_3Q_8$ are shown in Fig. 7, while for the remaining systems are shown in Ref. [49]

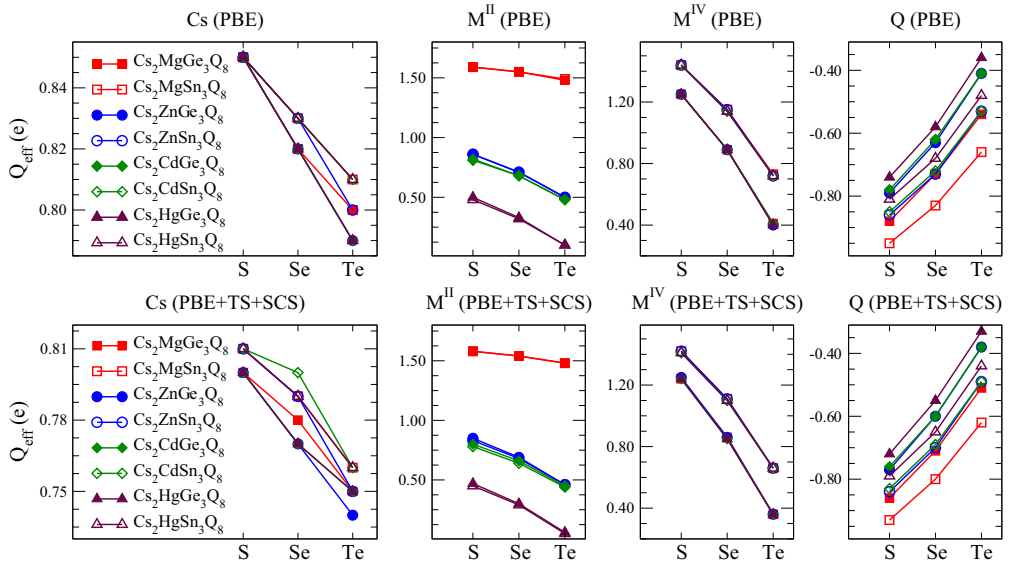

FIG. 5. Average Bader effective charges of each chemical species for the $Cs_2M^{II}M_3^{IV}Q_8$ compounds. Results in the upper row were obtained with PBE, while the bottom row shows results obtained with PBE+TS+SCS.

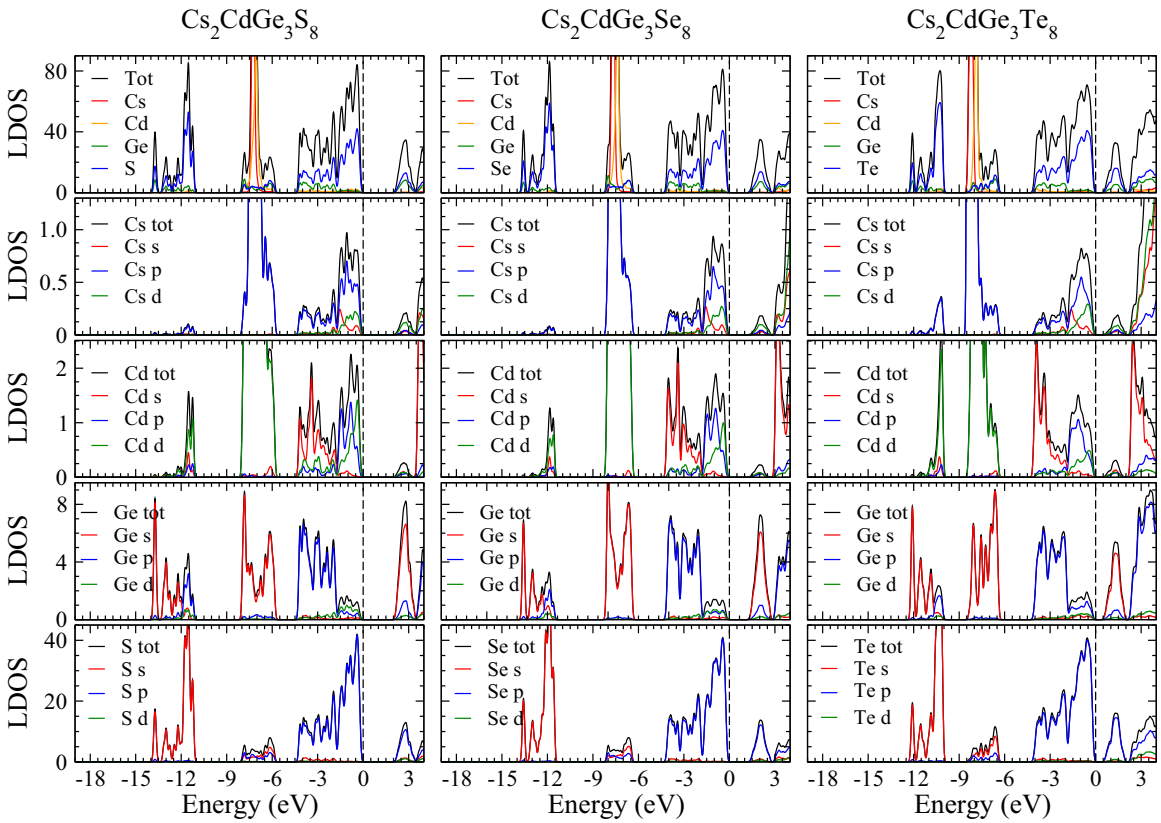

FIG. 6. DFT-PBE density of states of $Cs_2CdGe_3Q_8$, Q = S, Se, Te calculated at the PBE equilibrium geometry. The top of the valence band is shifted to the zero energy.

(Figs. S13 to S18). The valence bands are flat and the valence band maximum (VBM) is located at the Γ point for some compounds, while for the remaining it is located along the lines $\Gamma-Y$, $\Gamma-Z$, or $\Gamma-T$ with energy differences smaller than 10–35 meV compared with the Γ point. On the other hand, the conduction bands are more dispersive, with the conduction band minimum (CBM) located at the Γ point for all the structures with exception of $Cs_2M^{II}Ge_3Te_8$ (M^{II} = Mg,

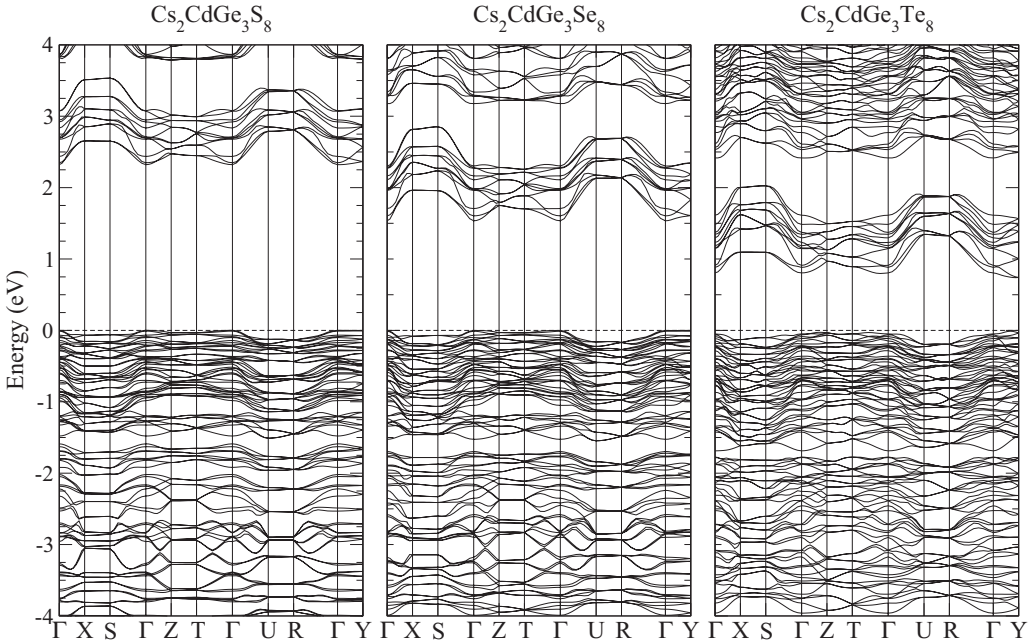

FIG. 7. DFT-PBE band structures of the $Cs_2CdGe_3Q_8$ compounds for Q = S, Se, and Te in the orthorhombic crystal structure. The top of the valence band is shifted to zero energy.

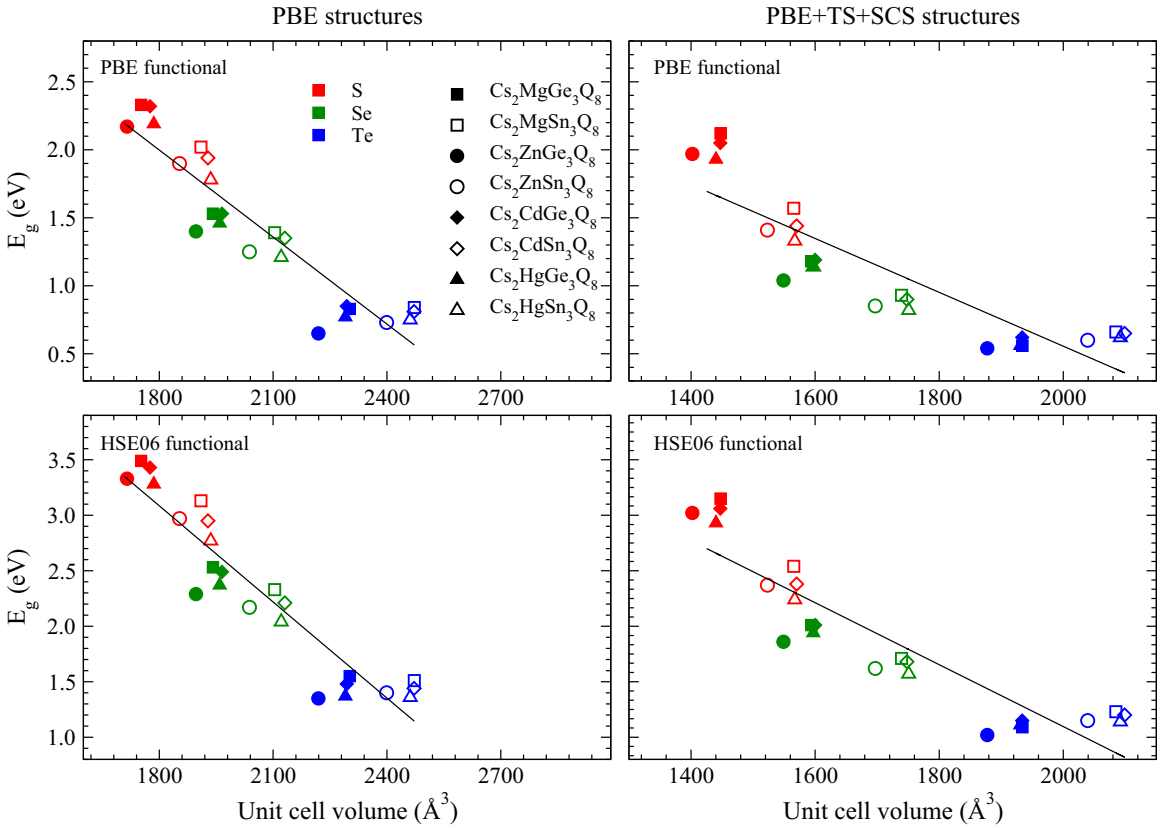

FIG. 8. Band gaps calculated at the Γ point as a function of unit cell volume for the $Cs_2M^{II}M_3^{IV}Q_8$ compounds. Results in the first column correspond to PBE crystal structures, while those in the second column were obtained for PBE+TS+SCS crystal structures. The band gaps were calculated with PBE functional (first row) and HSE06 functional (second row).

Zn, Cd, Hg) that occur at the line $\Gamma-Y$ with the minimum 25–70 meV below the energy at the Γ point. Thus, due to the small energy differences, few compounds have a small indirect nature in the band gap, while most of them have a direct band gap at the Γ point. It can be seen that the dispersion of the lowest energy conduction bands can be controlled by the selection of the M^{IV} or Q species. The substitutions of Ge by Sn, and S or Te by Se result in more dispersive bands.

Previous LDA calculations [21] underestimated the band gaps of the 11 $Cs_2M^{II}M_3^{IV}Q_8$ compounds by about 24%–48%. As expected, our PBE results for the 24 compounds follow also the same trend, i.e., underestimates the band gaps by about 25%–53%. The PBE+TS+SCS functional does not change this trend as the vdW correction only affects directly the structure, which in turn affects the eigenvalues. To improve the description, we calculated the energy band gap using the HSE06 functional employing the PBE and PBE+TS+SCS orthorhombic crystal structures. All the PBE, PBE+TS+SCS, and HSE06 band gaps at the Γ point are shown in Fig. 8 as a function of the equilibrium volume, and the numerical results are listed in Table S10 (Ref. [49]). As expected, HSE06 improves the agreement with the experimental results, i.e., for the 11 systems characterized by experimental techniques, it reduces the average relative error to about 7.5% and 14.3% employing the PBE and PBE+TS+SCS crystal structures, respectively.

For all functionals, we found that the band gap decreases almost linearly by increasing the equilibrium volume, and there is a large diversity of band-gap values among the studied compounds, e.g., from 1.35–3.49 eV with HSE06 using the PBE structures. Thus the present results suggest that the band gap can be tuned by a proper selection of the anion and cations in the $Cs_2M^{II}M_3^{IV}Q_8$ family. The anions play the main role in the variation of the band gap, i.e., the band gap increases almost linearly by decreasing the anion atomic number. This behavior is well known among chalcogenide compounds [10,50,59], and it is associated with the relative increasing of Q *p*-states energy, leading to a higher VBM and narrowing the band gap.

The band gap is also decreased when Sn replaces Ge, except for the compounds containing Te, in which the differences are smaller than 0.15 eV. Based on the higher energy of the Sn *s* states, the CBM energy is expected to increase, widening the band gap. However, the increase in the volume is known to descrease the band gap in semiconductors [60], and therefore this effect leads to the observed behavior, indicating that in these compounds it gets weaker going from S to Te. Furthermore, we notice that the M^{II} cations do not affect significantly the band gap for a given anion Q and cation M^{IV} because of their low contribution to electronic band edge states and small effect on the unit cell volume.

E. Optical properties

To investigate the chalcogenides optical properties, we calculated the optical transitions matrix elements, which were used to obtain the dielectric function [61,62], and then

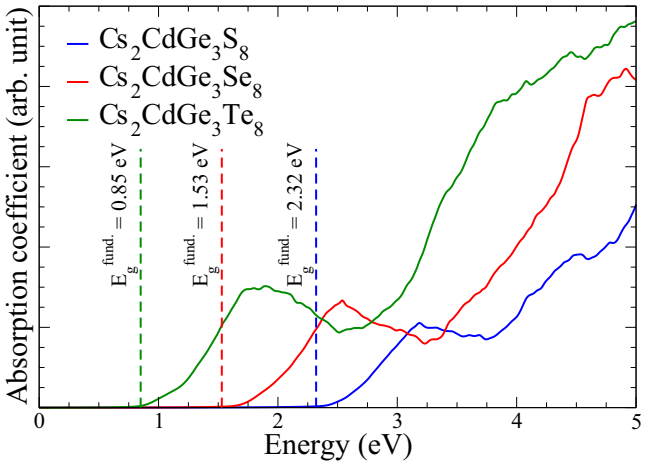

FIG. 9. Absorption coefficient of the $CsCdGe_3Q_8$ compounds obtained with PBE. Vertical dashed lines indicate the fundamental Γ point band gap of each compound calculated with PBE.

the absorption coefficients [63]. The optical band gap was determined by analysis of transition matrix elements at the Γ point, as all compounds have a direct or nearly direct band gap at the Γ point. The existence of a difference between the optical and fundamental band gap, generated by forbidden optical transitions, is a very important property to design materials for applications such as solar cells and flat panel displays, as observed in the transparent conducting oxides (TCOs) [64–66]. Our analysis for 6 representative compounds ($Cs_2CdGe_3S_8$, $Cs_2CdGe_3Se_8$, $Cs_2CdGe_3Te_8$, $Cs_2CdSn_3S_8$, $Cs_2MgGe_3S_8$, and $Cs_2MgSn_3Se_8$) shows that there is practically no difference between the optical and fundamental band gap, i.e., differences are less than 0.1 eV based on the analysis of the magnitude of the transition matrix elements.

Recently, three conditions were suggested to control the magnitude of the transition matrix elements in the context of TCOs [66], which defines the disparity between fundamental and optical band gaps. (i) The inversion symmetry defines the parity of the wave function, which turns all transitions between the electronic states with the same parity forbidden at the Γ point. The orthorhombic structure for the 24 compounds does not have inversion symmetry, and hence, the optical transitions are not forbidden. (ii) The orthorhombic lattice with space group $P2_12_12_1$ belongs to the character table D_2, and hence, only transitions between states that belong to the same representation are forbidden by the selection rule of group theory. All the remaining transitions, which are composed by the combination of A, B_1, B_2, and B_3 will be allowed for a specific direction (x, y, or z). (iii) The existence of a large number of bands at Γ point with similar energy in the vicinity of VBM and CBM increases the number of optical transitions, reducing the possibility of a large energy difference between a forbidden transition and the first allowed transition. Therefore this analysis can explain the difference of less than 0.1 eV between the fundamental and optical band gap for selected compounds, which can be extended for all 24 studied compounds.

These results also can be observed in the absorption coefficient curve, calculated with PBE functional and shown in the Fig. 9 for $CsCdGe_3Q_8$ (the remaining systems have the same behavior, Figs. S19 and S20 in Ref. [49]). The absorption curve starts in an energy very close to the fundamental band gap, indicating that there is no difference between optical and fundamental band gap. When the photon energy increases, the absorption curve produces a shoulder format before it starts to increase again. The existence of this shoulder and its length are consequences of the energy gap between successive unoccupied bands at the same **k** point in the upper region of the conduction band, as shown in Fig. 7.

IV. CONCLUSIONS

We performed DFT calculations within the PBE, PBE+TS+SCS, and HSE06 functionals to study the structural, energetic, electronic, and optical properties of the 24 chalcogenide $Cs_2M^{II}M_3^{IV}Q_8$ compounds (M^{II} =Mg, Zn, Cd, Hg; M^{IV} = Ge, Sn; Q = S, Se, Te) in the othorhombic crystal structure. The equilibrium volume increases almost linearly by increasing the atomic radius of the chalcogen atoms, namely, from S to Te. The atomic radius of the M^{II} and M^{IV} cations also affects the equilibrium volume. As expected, the attractive nature of the vdW correction decreases the equilibrium lattice parameters, in particular, the interlayer separation between the $Cs_2M^{II}M_3^{IV}Q_8$ layers. We found that the interlayer binding energy per unit of area with the vdW correction is similar to the results obtained for several different vdW layered materials such as graphite, etc. From the analysis of the Bader charges, we found that the Coulomb interactions among the cation and anions play an important role in the magnitude of the cohesive energy, which decreases in absolute value from S to Te. The band gaps obtained with the hybrid HSE06 functional are in good agreement with measured results (11 systems), and hence, our results provide excellent predictions for the remaining systems. Furthermore, we confirm that the band gaps vary substantially among the different compounds (e.g., from 1.3–3.5 eV) and exhibit an approximate linear correlation with unit cell volume, which can be explained by the increase in the relative energy of the Q p states with increasing atomic radius from S to Te.

ACKNOWLEDGMENTS

We thank the National Counsel of Technological and Scientific Development (CNPq), Process No. 470416/2013-0, the Coordination for the Improvement of Higher Level education (CAPES), the São Paulo Research Foundation (FAPESP), Process No. 2013/21045-2 and No. 2014/25924-3, and the infrastructure provided to our computer cluster by the São Carlos Center of Informatics, University of So Paulo.

[1] A. Morales-Acevedo, Sol. Energy **80**, 675 (2006).
[2] M. Wuttig and N. Yamada, Nat. Mater. **6**, 824 (2007).
[3] A. K. Geim and I. V. Grigorieva, Nature (London) **499**, 419 (2013).
[4] S. D. Feldman, R. T. Collins, V. Kaydanov, and T. R. Ohno, Appl. Phys. Lett. **85**, 1529 (2004).
[5] L. Zhang, J. L. F. Da Silva, J. Li, Y. Yan, T. A. Gessert, and S.-H. Wei, Phys. Rev. Lett. **101**, 155501 (2008).

[6] J. L. F. Da Silva, S.-H. Wei, J. Zhou, and X. Wu, Appl. Phys. Lett. **91**, 091902 (2007).

[7] I. Repins, M. A. Contreras, B. Egaas, C. DeHart, J. Scharf, C. L. Perkins, B. To, and R. Noufi, Prog. Photovoltaics Res. Appl. **16**, 235 (2008).

[8] T. K. Todorov, K. B. Reuter, and D. B. Mitzi, Adv. Mater. **22**, E156 (2010).

[9] J. Androulakis, S. C. Peter, H. Li, C. D. Malliakas, J. A. Peters, Z. Liu, B. W. Wessels, J.-H. Song, H. Jin, A. J. Freeman, and M. G. Kanatzidis, Adv. Mater. **23**, 4163 (2011).

[10] S. Johnsen, S. C. Peter, S. L. Nguyen, J.-H. Song, H. Jin, A. J. Freeman, and M. G. Kanatzidis, Chem. Mater. **23**, 4375 (2011).

[11] H. Li, C. D. Malliakas, J. A. Peters, Z. Liu, J. Im, H. Jin, C. D. Morris, L.-D. Zhao, B. W. Wessels, A. J. Freeman, and M. G. Kanatzidis, Chem. Mater. **25**, 2089 (2013).

[12] S. M. Islam, S. Vanishri, H. Li, C. C. Stoumpos, J. A. Peters, M. Sebastian, Z. Liu, S. Wang, A. S. Haynes, J. Im, A. J. Freeman, B. Wessels, and M. G. Kanatzidis, Chem. Mater. **27**, 370 (2015).

[13] W. Khan and S. Goumri-Said, RSC Adv. **5**, 9455 (2015).

[14] T. K. Bera, J.-H. Song, A. J. Freeman, J. I. Jang, J. B. Ketterson, and M. G. Kanatzidis, Angew. Chem. Int. Ed. **47**, 7828 (2008).

[15] T. K. Bera, J. I. Jang, J.-H. Song, C. D. Malliakas, A. J. Freeman, J. B. Ketterson, and M. G. Kanatzidis, J. Am. Chem. Soc. **132**, 3484 (2010).

[16] T. Kyratsi, K. Chrissafis, J. Wachter, K. M. Paraskevopoulos, and M. G. Kanatzidis, Adv. Mater. **15**, 1428 (2003).

[17] J.-W. Park, S. H. Baek, T. D. Kang, H. Lee, Y.-S. Kang, T.-Y. Lee, D.-S. Suh, K. J. Kim, C. K. Kim, Y. H. Khang, J. L. F. Da Silva, and S.-H. Wei, Appl. Phys. Lett. **93**, 021914 (2008).

[18] J. L. F. Da Silva, A. Walsh, and H. Lee, Phys. Rev. B **78**, 224111 (2008).

[19] J. L. F. Da Silva, A. Walsh, S.-H. Wei, and H. Lee, J. Appl. Phys. **106**, 113509 (2009).

[20] Z. H. Fard and M. G. Kanatzidis, Inorg. Chem. **51**, 7963 (2012).

[21] C. D. Morris, H. Li, H. Jin, C. D. Malliakas, J. A. Peters, P. N. Trikalitis, A. J. Freeman, B. W. Wessels, and M. G. Kanatzidis, Chem. Mater. **25**, 3344 (2013).

[22] T. Bučko, J. Hafner, S. Lebègue, and J. G. Ángyán, J. Phys. Chem. A **114**, 11814 (2010).

[23] A. Tkatchenko, L. Romaner, O. T. Hofmann, E. Zojer, C. Ambrosch-Draxl, and M. Scheffler, MRS Bull. **35**, 435 (2010).

[24] V. V. Gobre and A. Tkatchenko, Nat. Commun. **4**, 2341 (2013).

[25] C. R. C. Rêgo, L. N. Oliveira, P. Tereshchuk, and J. L. F. Da Silva, J. Phys.: Condens. Matter **27**, 415502 (2015).

[26] P. Hohenberg and W. Kohn, Phys. Rev. **136**, B864 (1964).

[27] W. Kohn and L. J. Sham, Phys. Rev. **140**, A1133 (1965).

[28] J. P. Perdew, K. Burke, and M. Ernzerhof, Phys. Rev. Lett. **77**, 3865 (1996).

[29] M. Fuchs, J. L. F. Da Silva, C. Stampfl, J. Neugebauer, and M. Scheffler, Phys. Rev. B **65**, 245212 (2002).

[30] J. L. F. Da Silva, C. Stampfl, and M. Scheffler, Surf. Sci. **600**, 703 (2006).

[31] P. Haas, F. Tran, and P. Blaha, Phys. Rev. B **79**, 085104 (2009).

[32] J. L. F. Da Silva, C. Stampfl, and M. Scheffler, Phys. Rev. B **72**, 075424 (2005).

[33] J. L. F. Da Silva and C. Stampfl, Phys. Rev. B **76**, 085301 (2007).

[34] J. L. F. Da Silva and C. Stampfl, Phys. Rev. B **77**, 045401 (2008).

[35] A. Tkatchenko, R. A. DiStasio, R. Car, and M. Scheffler, Phys. Rev. Lett. **108**, 236402 (2012).

[36] T. Bučko, S. Lèbegue, J. Hafner, and J. G. Ángyán, Phys. Rev. B **87**, 064110 (2013).

[37] J. P. Perdew and M. Levy, Phys. Rev. Lett. **51**, 1884 (1983).

[38] T. L. Bahers, M. Rérat, and P. Sautet, J. Phys. Chem. C **118**, 5997 (2014).

[39] J. Heyd, G. E. Scuseria, and M. Ernzerhof, J. Chem. Phys. **118**, 8207 (2003).

[40] J. Heyd and G. E. Scuseria, J. Chem. Phys. **121**, 1187 (2004).

[41] J. Heyd, G. E. Scuseria, and M. Ernzerhof, J. Chem. Phys. **124**, 219906 (2006).

[42] A. V. Krukau, O. A. Vydrov, A. F. Izmaylov, and G. E. Scuseria, J. Chem. Phys. **125**, 224106 (2006).

[43] P. E. Blöchl, Phys. Rev. B **50**, 17953 (1994).

[44] G. Kresse and D. Joubert, Phys. Rev. B **59**, 1758 (1999).

[45] G. Kresse and J. Hafner, Phys. Rev. B **48**, 13115 (1993).

[46] G. Kresse and J. Furthmüller, Phys. Rev. B **54**, 11169 (1996).

[47] J. L. F. Da Silva, M. V. Ganduglia-Pirovano, J. Sauer, V. Bayer, and G. Kresse, Phys. Rev. B **75**, 045121 (2007).

[48] C. Kittel, *Introduction to Solid State Physics*, 7th ed. (Wiley, New York, 1996).

[49] See Supplemental Material at http://link.aps.org/supplemental/10.1103/PhysRevB.93.165205 for numerical tables of the lattice parameters, cohesive energies, interlayer binding energies, average Bader charges and energy band gaps. Furthemore, we report also density of states, band structures, and optical properties for all systems.

[50] H.-R. Liu, S. Chen, Y.-T. Zhai, H. J. Xiang, X. G. Gong, and S.-H. Wei, J. Appl. Phys. **112**, 093717 (2012).

[51] A. Tkatchenko and M. Scheffler, Phys. Rev. Lett. **102**, 073005 (2009).

[52] R. Hoppe, Z. Kristallogr. **150**, 23 (1979).

[53] J. L. F. Da Silva, J. Appl. Phys. **109**, 023502 (2011).

[54] C. H. Holbrow, J. N. Lloyd, J. C. Amato, E. Galvez, and M. E. Parks, *Hard-Sphere Atoms* (Springer New York, 2010), p. 109.

[55] T. Björkman, A. Gulans, A. V. Krasheninnikov, and R. M. Nieminen, Phys. Rev. Lett. **108**, 235502 (2012).

[56] R. F. W. Bader, *Atoms in Molecules: A Quantum Theory*, International Series of Monographs on Chemistry (Clarendon Press, Oxford, 1994).

[57] E. Sanville, S. D. Kenny, R. Smith, and G. Henkelman, J. Comput. Chem. **28**, 899 (2007).

[58] L. Pauling, *The Nature of the Chemical Bond* (Cornell University Press, Ithaca, 1960).

[59] Y.-Y. Sun, M. L. Agiorgousis, P. Zhang, and S. Zhang, Nano Lett. **15**, 581 (2015).

[60] Y.-H. Li, X. G. Gong, and S.-H. Wei, Phys. Rev. B **73**, 245206 (2006).

[61] B. Adolph, J. Furthmüller, and F. Bechstedt, Phys. Rev. B **63**, 125108 (2001).

[62] M. Gajdoš, K. Hummer, G. Kresse, J. Furthmüller, and F. Bechstedt, Phys. Rev. B **73**, 045112 (2006).

[63] D. Segev and S.-H. Wei, Phys. Rev. B **71**, 125129 (2005).

[64] B. G. Lewis and D. C. Paine, MRS Bull. **25**, 22 (2000).

[65] A. Walsh, J. L. F. Da Silva, S.-H. Wei, C. Körber, A. Klein, L. F. J. Piper, A. DeMasi, K. E. Smith, G. Panaccione, P. Torelli, D. J. Payne, A. Bourlange, and R. G. Egdell, Phys. Rev. Lett. **100**, 167402 (2008).

[66] F. P. Sabino, R. Besse, L. N. Oliveira, S.-H. Wei, and J. L. F. Da Silva, Phys. Rev. B **92**, 205308 (2015).